Utilizing Frequency- and Time Domain Methods for the Operational Modal Analysis of a Bridge

Markus Klötzer, B.Sc., Dr. techn. Franz-Josef Falkner (Supervisor)

***Abstract*—Operational modal analysis (OMA) serves as a tool to characterize the dynamic properties of mechanical structures. During this project, methods to compute the modal parameters in time- and frequency domain applied to a steel plate and a bridge are explored. The theoretical backgrounds of OMA as a method for system identification without known excitation are explored along an evaluation of strengths and weaknesses of different time- and frequency domain approaches, such as frequency domain decomposition (FDD) and stochastic subspace identification (SSI).**

For validation, an experiment is set up in a laboratory environment to eliminate potentially disturbing real-world influences. This test setup consists of a simple mechanical structure (steel plate) being excited by loads similar to operational forces for the output accelerations to be processed. The resulting modal parameters (modal damping, natural frequencies and their associated mode shapes) are then compared to the simulation results of the same part. Additionally, experiments are conducted on a bridge, where OMA is applied most commonly due to it not intervening with normal bridge traffic. The results are then validated with experimental modal analysis (EMA) performed on the same structure.

***Index Terms*—Operational Modal Analysis, Structural Dynamics, System Identification, Infrastructure**

I. Introduction

MODAL analysis describes a type of system identification method where the dynamical parameters of physical systems are extracted. These modal parameters give useful information about the system's behaviour and help to avoid or target effects like resonance.

There are multiple ways of extracting the dynamical properties or modal parameters of a mechanical system. These properties include the natural frequencies, modal damping ratios as well as mode shapes and can be calculated analytically, by means of the finite elements (FE) method or with the use of EMA. The third approach utilizes vibration measurements on a structure excited by a known input force. The modal parameters are then calculated by relating the input force to the measured output quantities.

Another experimental approach is OMA, where the structure is not excited artificially, but the vibration measurements of the structure are taken during regular operation. Since the input quantities are unknown, the basic assumption for all OMA methods is that the operational loads provide excitation at every frequency up to a certain value. This form of excitation is called broadband loading [1] and is different to white noise, in that not all frequencies are loaded equally, so the input forces are not stochastic but in most cases an accumulation of a multitude of different operational loads. The processing methods, however, all assume the input to be fully random.

For EMA the methods of excitation typically include impacts by the use of a hammer, electromechanical or eccentric shakers, all typically equipped with a force sensor for the input quantities to be included in the computation of modal parameters. During OMA, however, the excitation of the structure stems from a multitude of different sources. According to [1], infrastructure buildings are typically affected by wind, traffic, be it by foot or other means, water and sound, while mechanical parts are generally exposed to machine vibrations and impacts.

OMA provides some benefits over EMA, in that no controlled input needs to be provided. Operational loads are also not beneficial to the results of EMA since these forces are not accounted for in data processing, leading to the structure having to be analysed in a more controlled environment. Infrastructure needs to be closed off from traffic or machines need to be disassembled for the parts to be tested. Large buildings, though, cannot be isolated fully from the surrounding influences, biasing results from EMA.

II. State of the Art

The main methods of OMA explored are the FDD and SSI. The basis for both approaches is the assumption of white noise force inputs over a broad

frequency range leading to the excitation of all modes within this frequency band.

A. Frequency Domain Decomposition

According to [1] the time response of a system

$$\vec{y}(t) = \mathbf{\Phi}\vec{q}(t) = \sum_{m=1}^{M} \vec{\phi}_m \cdot q_m(t) \tag{1}$$

can be described as the product of mode shapes $\vec{\phi}_n$, within the mode shape matrix $\mathbf{\Phi}$, and the modal coordinates $q_n(t)$, arranged in the modal coordinate vector $\vec{q}(t)$, with $m = 1, 2, \cdots, M-1, M$ determining the number of modal coordinates. The correlation

$$\boldsymbol{R}_y(\tau) = E[\vec{y}(t)\vec{y}^T(t+\tau)] \tag{2}$$

of the response is formed, where $E[\,]$ denotes the expected value of the function. Combining equations (1) and (2) leads to

$$\boldsymbol{R}_y = \mathbf{\Phi}\boldsymbol{R}_q(\tau)\mathbf{\Phi}^T = \mathbf{\Phi}E[\vec{q}(t)\vec{q}^T(t+\tau)]\mathbf{\Phi}^T\,. \tag{3}$$

This can be done since the mode shape matrix $\mathbf{\Phi}$ is not a function of time. Equation (3) can now be transformed into frequency domain by applying the Fourier transform $\mathcal{F}\{\}$ on the correlations

$$\boldsymbol{G}_y(f) = \mathcal{F}\{\boldsymbol{R}_y\} = \mathbf{\Phi}\mathcal{F}\{\boldsymbol{R}_q\}\mathbf{\Phi}^T\,. \tag{4}$$

$\boldsymbol{G}_y(f)$ is the spectral density (SD) of the structure's output. The equation (4) can be rewritten as

$$\boldsymbol{G}_y(f) = \mathbf{\Phi}\boldsymbol{G}_q(f)\mathbf{\Phi}^H = \mathbf{\Phi}[g_m^2(f)]\mathbf{\Phi}^H \tag{5}$$

where $g_m^2(f)$ are the auto spectral densities of the modal coordinates. Since the mode shape matrix is complex, the hermitian, or conjugate transpose H is used. Equation (5) is equivalent to the singular value decomposition of a quadratic matrix.

$$\boldsymbol{G}_y(f) = \boldsymbol{U}\boldsymbol{S}\boldsymbol{U}^H = \boldsymbol{U}[s_m^2(f)]\boldsymbol{U}^H \tag{6}$$

This leads to the conclusion that applying the singular value decomposition on the SD matrix of the measured system output can provide us with the mode shape matrix $\mathbf{\Phi} = \boldsymbol{U}$ and the autospectral densities $\boldsymbol{G}_q$ of the modal coordinates positioned at the diagonal of $\boldsymbol{S}$. However, it is important to note that this operation is only performed under the assumption that the mode shapes are uncorrelated. This means that the mode shape matrix $\mathbf{\Phi}$ is unitary, meaning that the columns are completely orthogonal to each other. In reality this is not the case, which is why the FDD delivers only an approximation of the modes. The singular value decomposition arranges $\boldsymbol{S}$ in order of magnitude. To identify the frequencies of interest the largest singular value is plotted over all frequencies, so that the peaks can be picked. To get the mode shape at the frequency of interest, f_j, the first column of $\boldsymbol{U}(f_j)$ is extracted, due to it having the highest influence on the system response because it is multiplied with the largest singular value. This method is patented to [2].

To estimate the damping values at each frequency of interest, the enhanced frequency domain decomposition (EFDD) is used as described in [3]. Over a certain bandwidth around one natural frequency the according mode shape dominates. Correlating the mode shape $\vec{\phi}_1$ at f_j to all the other mode shapes $\vec{\phi}_2$ via the modal assurance criterion (MAC) [4],

$$\text{MAC}(\vec{\phi}_1, \vec{\phi}_2) = \frac{|\vec{\phi}_1^H \vec{\phi}_2|^2}{(\vec{\phi}_1^H \vec{\phi}_1)(\vec{\phi}_2^H \vec{\phi}_2)}\,, \tag{7}$$

over the complete spectrum can isolate the peak of interest by it having to surpass a threshold. The singular values over this bandwidth are determined to be the SD of one single degree of freedom (SDOF) system. This isolated peak is then re-transformed into the time domain, leading to the autocorrelation function of the peak. The natural frequency of said SDOF autocorrelation function can now be determined by identifying the frequency of its zero-crossings. The logarithmic decrement

$$\delta = \frac{2}{k}\ln\left(\frac{r_0}{|r_k|}\right)\,, \tag{8}$$

with r_0 being the initial and r_k being the k^{th} extreme of the autocorrelation function, determines the damping ratio ζ via

$$\zeta = \frac{\delta}{\sqrt{\delta^2 + 4\pi^2}}\,. \tag{9}$$

In practice it is common [3] to perform a linear fit using the least squares method on $k\delta$ and $2\ln(|r_k|)$, which returns an estimate for the logarithmic decrement.

B. Stochastic Subspace Identification

Since the amount of different identification algorithms for linear time invariant (LTI) systems using the subspace method seems endless, the focus is placed on the covariance driven stochastic subspace identification (SSI-COV), which is used during the experiments performed for the purposes of this Master's project.

SSI-COV, according to [5], is based on estimating the discrete system matrix $\boldsymbol{A}$ and the output influence

matrix $\boldsymbol{C}$ by means of the output covariances $\boldsymbol{R}_{yy}$ within the Toeplitz matrix $\boldsymbol{T}_i$, which is the arranged in the form of

$$\boldsymbol{T}_i = \begin{bmatrix} \boldsymbol{R}_{yy,i} & \boldsymbol{R}_{yy,i-1} & \cdots & \boldsymbol{R}_{yy,1} \\ \boldsymbol{R}_{yy,i+1} & \boldsymbol{R}_{yy,i} & \cdots & \boldsymbol{R}_{yy,2} \\ \boldsymbol{R}_{yy,i+2} & \boldsymbol{R}_{yy,i+1} & \cdots & \boldsymbol{R}_{yy,3} \\ \vdots & \vdots & \ddots & \vdots \\ \boldsymbol{R}_{yy,2i-1} & \boldsymbol{R}_{yy,2i-2} & \cdots & \boldsymbol{R}_{yy,i} \end{bmatrix} . \quad (10)$$

Basically the Toeplitz matrix contains all output covariance matrices shifted by up to $2i-1$. Substituting the shifted covariances with

$$\boldsymbol{R}_{yy,i} = \boldsymbol{C}\boldsymbol{A}^{i-1}\boldsymbol{R}_{xy} \quad (11)$$

shows that, conveniently, the system matrix $\boldsymbol{A}$ and the output influence matrix $\boldsymbol{C}$, together with the covariance $\boldsymbol{R}_{xy}$ between states $\vec{x}$ and outputs $\vec{y}$ are contained within the Toeplitz matrix, which in turn can be calculated from the measurement data only. To extract $\boldsymbol{A}$ and $\boldsymbol{C}$, $\boldsymbol{T}_i$ can be split up into the observability matrix

$$\boldsymbol{\Gamma}_i = \begin{bmatrix} \boldsymbol{C} \\ \boldsymbol{C}\boldsymbol{A} \\ \vdots \\ \boldsymbol{C}\boldsymbol{A}^{i-1} \end{bmatrix} \quad (12)$$

and a reverse variation of the controllability matrix for stochastic systems

$$\boldsymbol{\Delta}_i = \begin{bmatrix} \boldsymbol{A}^{i-1}\boldsymbol{R}_{\boldsymbol{xy}} & \cdots & \boldsymbol{A}\boldsymbol{R}_{\boldsymbol{xy}} & \boldsymbol{R}_{\boldsymbol{xy}} \end{bmatrix} \quad (13)$$

according to

$$\boldsymbol{T}_i = \boldsymbol{\Gamma}_i \boldsymbol{\Delta}_i . \quad (14)$$

Decomposing the Toeplitz matrix into $\boldsymbol{\Gamma}_i$ and $\boldsymbol{\Delta}_i$ is achieved by utilizing the singular value decomposition

$$\boldsymbol{T}_i = \boldsymbol{U}\boldsymbol{S}\boldsymbol{V}^T = \begin{bmatrix} \boldsymbol{U}_1 & \boldsymbol{U}_2 \end{bmatrix} \begin{bmatrix} \boldsymbol{S}_1 & \boldsymbol{0} \\ \boldsymbol{0} & \boldsymbol{S}_2 \end{bmatrix} \begin{bmatrix} \boldsymbol{V}_1^T \\ \boldsymbol{V}_2^T \end{bmatrix} . \quad (15)$$

Only the non-zero entries of the singular values, $\boldsymbol{S}_1$, and the according singular vectors $\boldsymbol{U}_1$ and $\boldsymbol{V}_1^T$ are used for the calculation of $\boldsymbol{\Gamma}_i$, hence

$$\boldsymbol{T}_i = \boldsymbol{U}_1 \boldsymbol{S}_1 \boldsymbol{V}_1^T = \boldsymbol{\Gamma}_i \boldsymbol{\Delta}_i . \quad (16)$$

Expanding equation (16) with the weighting matrix $\boldsymbol{W}$, which is then replaced by a unit matrix, and splitting it into

$$\boldsymbol{\Gamma}_i = \boldsymbol{U}_1 \boldsymbol{S}_1^{1/2} \boldsymbol{W} = \boldsymbol{U}_1 \boldsymbol{S}_1^{1/2} \quad (17)$$

and

$$\boldsymbol{\Delta}_i = \boldsymbol{W}^{-1} \boldsymbol{S}_1^{1/2} \boldsymbol{V}_1^T = \boldsymbol{S}_1^{1/2} \boldsymbol{V}_1^T \quad (18)$$

is done due to the similarity to equation (14).

According to [6], $\boldsymbol{C}$ can be determined directly from the observability matrix, by extracting its first block. The methods for determining $\boldsymbol{A}$ vary. One approach of extracting the system matrix is the method proposed by [7] solving

$$\boldsymbol{A} = \boldsymbol{\Gamma}_1^{+} \boldsymbol{\Gamma}_2 , \quad (19)$$

where $\boldsymbol{\Gamma}_1^{+}$ denotes the pseudoinverse of all block rows of the observability matrix except the last, while $\boldsymbol{\Gamma}_2$ denotes all block rows except the first one. This is based on

$$\boldsymbol{\Gamma}_2 = \begin{bmatrix} \boldsymbol{C}\boldsymbol{A} \\ \boldsymbol{C}\boldsymbol{A}^2 \\ \vdots \\ \boldsymbol{C}\boldsymbol{A}^i \end{bmatrix} = \boldsymbol{A}\boldsymbol{\Gamma}_1 = \boldsymbol{A} \begin{bmatrix} \boldsymbol{A} \\ \boldsymbol{C}\boldsymbol{A} \\ \vdots \\ \boldsymbol{C}\boldsymbol{A}^{i-1} \end{bmatrix} . \quad (20)$$

According to [6] the modal parameters for each order can be extracted by performing the eigenvalue decomposition of the System matrix $\boldsymbol{A}$ using

$$\boldsymbol{A} = \boldsymbol{\Psi}_i \left[\mu_i\right] \boldsymbol{\Psi}_i^{-1} . \quad (21)$$

with $\boldsymbol{\Psi}_i$ being its eigenvectors and μ_i being the eigenvalues or poles of the discrete system. The continuous poles λ_i are calculated via

$$\lambda_i = \frac{ln(\mu_i)}{\Delta T} , \quad (22)$$

with ΔT being the sampling time. The natural frequency is now the absolute of the continuous pole

$$f_i = |\lambda_i| \quad (23)$$

and the according damping ratio ζ_i is

$$\zeta_i = \frac{Re(\lambda_i)}{|\lambda_i|} . \quad (24)$$

The mode shape vector $\vec{\phi}_i$ is the product of each eigenvector $\vec{\psi}_i$, which are the columns of $\boldsymbol{\Psi}_i$, and the output influence matrix

$$\vec{\phi}_i = \boldsymbol{C}\vec{\psi}_i . \quad (25)$$

Throughout those calculations i determines the order of the state space representation. It is common practice to iterate over different orders, extracting the model parameters for each and then checking for large deviations of modal parameters over the order changes. If the values vary strongly they are removed. Categorization into different kinds of stability are also common. Sometimes it is useful to know poles, which are stable in frequency, mode shapes, damping or all of the above. The results of the SSI are then typically plotted in a stability diagram.

According to [6] the algorithm speed is drastically increased by calculating $\boldsymbol{T}_i$ and performing the singular value decomposition for the highest order first and then varying the number of singular values and vectors according to the current order.

III. Objectives

The overall objective is to implement and apply OMA methods, be it SSI or FDD on real structures and validate the results to judge its field of application.

OMA is implemented by creating a custom program in Python. The goal is then to initially test OMA on a computationally generated dataset first to check for correctness of implementation. Furthermore, the goal of creating an experiment under laboratory conditions is set. For this purpose a steel plate with a hole is designed. Research on how to excite the structure in ways similar to the operational loads acting on a mechanical structure is done and applied. Since a detailed computer aided design (CAD) model is available, the results of OMA can be validated with simulation results stemming from ANSYS. The next objective during the project is to perform OMA on a bridge. To draw conclusions about the validity of results EMA is performed simultaneously with an impact hammer. But not only the validity of OMA will be determined; also, the the quality of results will show, which method performs better under certain circumstances.

IV. Methods

The methodologies employed in this project are designed to achieve a comprehensive understanding of the OMA-techniques described in section II and their practical applications. The approaches are structured to ensure thorough validation and comparison of the implemented methods each step of the way.

A. Implementation of OMA Techniques in Python

To create a reliable Python module containing all the necessary functions needed to process acceleration data provided from measurements, a dataset is generated. A system comprised of three masses, which are limited to one degree of freedom each, connected via springs and dampers are virtually excited by band-limited white noise. For testing purposes even harmonic components are introduced to check if the methods identify deterministic excitation wrongly as physical modes.

B. Experimental Setup and Validation of OMA on a Steel Plate

To create the ideal object, on which to test the effectiveness of OMA, a steel plate is designed in CAD. The 3d model is created and its dimensions adapted, so that most of the natural frequencies are well separated from each other. This is done by iteratively adapting the design and performing modal analysis in ANSYS. If the result is satisfactory, the plate, depicted in figure 1, is manufactured.

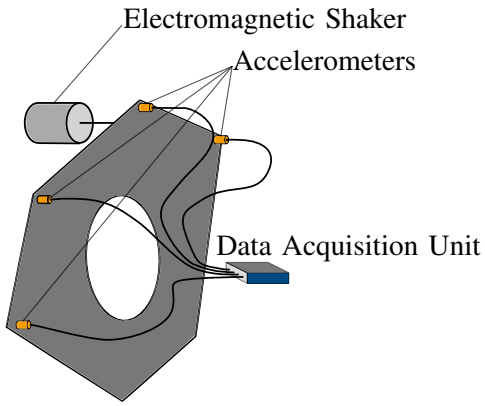

Fig. 1: OMA is performed on a steel plate with a multitude of different excitation methods.

The plate is subjected to random impacts, mimicking operational loads, while the shaker also provides deterministic excitation, which then need to be separated from the real natural frequencies during data processing, testing the anticipated limits of OMA.

C. Field Application on Tiflis Bridge

The next step is to apply all the knowledge gained from previous experiments on a structure, for which OMA is intended. The Tiflis Bridge, depicted in figure 2, in Innsbruck is spanned over the river Sill and is a steel construction measuring $42.8\,\mathrm{m}$ in length and $5.75\,\mathrm{m}$ in width.

Fig. 2: The Tiflis Bridge spans the river Sill and is used mainly for foot- and bike traffic.

The measurement setup is arranged in the following way. Roving sensors are positioned at two of the twelve modal points of interest near the railing of the bridge, depicted in figure 3, while one reference sensor is placed at a point, where no vibration node is expected. The reference sensor is used to scale the mode shapes, which is necessary since the excitation forces vary in strength over time, which means that the mode shapes of the reference sensors need to be scaled using the modal displacement of the reference coordinate. This approach enables the use less of sensors, without decreasing the resolution of the mode shapes.

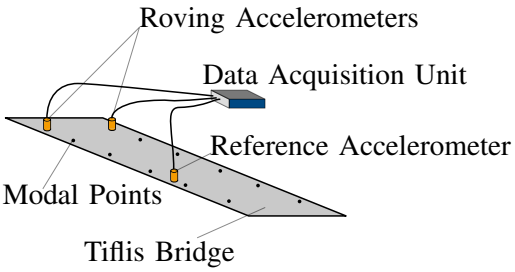

Fig. 3: The measurement setup used to perform OMA on the Tiflis bridge consists of two roving- and one reference sensor.

Traffic is limited, since it is closed of to cars and only bikers, pedestrians and the occasional scooter are allowed to pass. It is anticipated that the natural excitation is limited, leading to difficulties in data processing and extraction of modal parameters. Since EMA is performed at the same date at the same structure, a large impact hammer is used to artificially provide more excitation.

D. Field Application on Grenobler Bridge

A third field experiment is conducted, this time however on a bridge with more traffic. The Grenobler Bridge is displayed in figure 4 [8].

The increase in traffic intensity should, in theory at least, lead to a better excitation of modes. In contrast to the Tiflis Bridge the Grenobler bridge consists of two parts running parallel to each other. One part is intended for car traffic, while the other one is used for public transport via trams on the upper level, and foot- and bike traffic on the lower level. The bridge is supported on each end and via two pillars, each placed $28.5\,\mathrm{m}$ from the ends. The Distance between them is $44.0\,\mathrm{m}$. The width of the upper level is $6.5\,\mathrm{m}$ while the lower level width is $3.5\,\mathrm{m}$. The cross-section of the bridge is slightly asymmetric which should lead to horizontal displacements in the

Fig. 4: The object of interest is the part of the Grenobler Bridge used for public transport, foot- and bike traffic.

direction of the river. Hence triaxial sensors are used with their z-axis showing in vertical direction and the x-axis showing down the river. Two of these are placed directly in next to the railings, $47.6\,\mathrm{m}$ from the north-end. This placement slightly out of centre is chosen to avoid measuring at a vibration node, which for beam like structures are generally found in the middle between supports. The goal of this measurement is not to get the complete mode shape of the Grenobler bridge but to check if the excitation stemming from increased traffic, especially trams, leads to an improvement in the identification of modal parameters.

V. Results

A. Results of OMA on the Steel Plate

The measured data from the plate experiment is now used in both methods of OMA, with the singular value plot and the stability diagram depicted in figure 5.

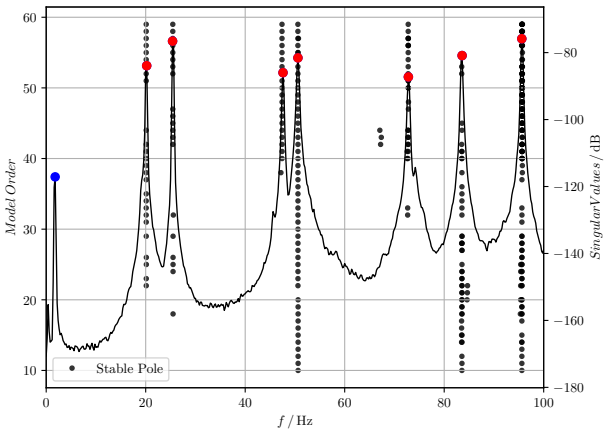

Fig. 5: The singular values and the poles extracted from the measurements performed on the plate.

The first peak (marked in blue) is not picked, since it does not correspond to any stable pole. Continuing with the modal analysis, both in frequency- and time domain, each dataset is evaluated separately and the frequency and damping results averaged. The results are listed in table I.

Method	f_n / Hz	ζ / %	MPC
SSI-COV	20.12	0.21	0.98
	25.48	0.07	0.99
	47.53	0.27	0.95
	50.70	0.32	0.98
	72.81	0.21	0.99
	83.58	0.14	0.99
	95.68	0.09	0.99
EFDD	20.13	0.24	0.99
	25.48	0.15	0.98
	47.54	0.15	0.79
	50.70	0.19	0.76
	72.82	0.16	0.99
	83.56	0.11	0.98
	95.67	0.08	0.99
FE	19, 28		
	24, 28		
	46, 94		
	49, 16		
	70, 47		
	82, 23		
	93, 43		

TABLE I: Comparison of modal parameters between OMA and FE performed on a steel plate.

ANSYS generally performs modal analysis without taking the damping properties of the material into consideration. Hence the modes are non-complex and damping values are not included in table I. The frequencies of the simulation result are within 1 Hz to 2 Hz of those determined by OMA, validating the method of output only modal analysis, at least under laboratory conditions.

B. Results of OMA on Tiflis Bridge

The measurement data of the recording sessions performed on the Tiflis Bridge is processed using the EFDD and SSI-COV. The resulting stability diagram over the singular value spectrum is depicted in figure 6.

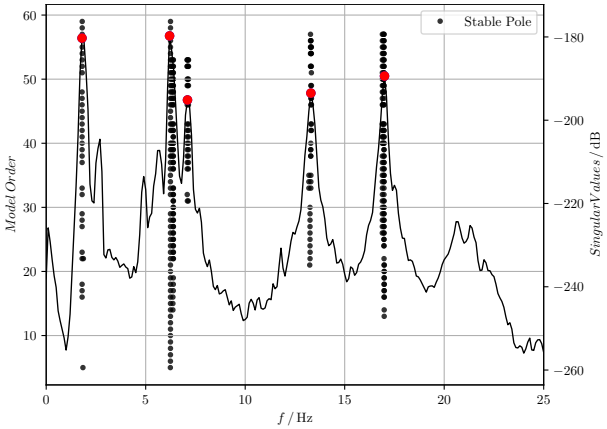

Fig. 6: The largest singular values and the stability diagram of the measurements performed on the Tiflis Bridge (session 1) are plotted up the the 25 Hz. The picked peaks are marked with red dots.

The highest peaks of the spectrum clearly indicate at least five physical modes up to 25 Hz and the stability diagram shows the same result. The resulting poles of the SSI-COV, however, slightly drift away from each other at higher orders. One reason could be the slight change in natural frequencies due to the bridge being very light and its mass changing with traffic in between the recordings of the individual datasets. A comparison of results between EMA and both OMA methods is shown in table II.

Method	f_n / Hz	ζ / %	MPC
SSI-COV	1.84	2.76	0.96
	6.34	0.67	1.00
	7.10	1.36	0.99
	13.31	0.48	1.00
EFDD	1.82	4.90	1.00
	6.35	0.10	0.99
	7.11	0.72	0.98
	13.31	0.74	1.00
	16.95	0.47	1.00
EMA	1.87	3.00	0.97
	6.07	0.45	0.87
	6.89	5.10	0.98
	13.34	0.77	0.94
	16.93	0.44	0.43

TABLE II: Comparison of modal parameters between OMA methods performed on the Tiflis Bridge.

The first five mode shapes of the Tiflis Bridge are displayed in figure 7.

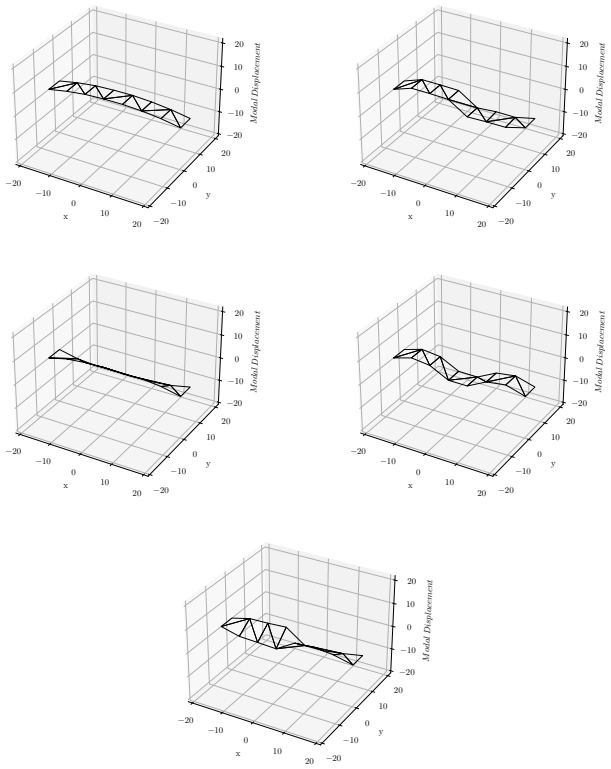

Fig. 7: The first five mode shapes of the Tiflis bridge.

The mode shapes of the Tiflis Bridge follow the expected pattern of one added vibration node at each new mode. The same goes for the torsional modes.

C. Results of OMA on Grenobler Bridge

The measurements of vertical and horizontal accelerations measured on the Grenobler Bridge result in the singular value spectrum and stability diagram depicted in figure 8.

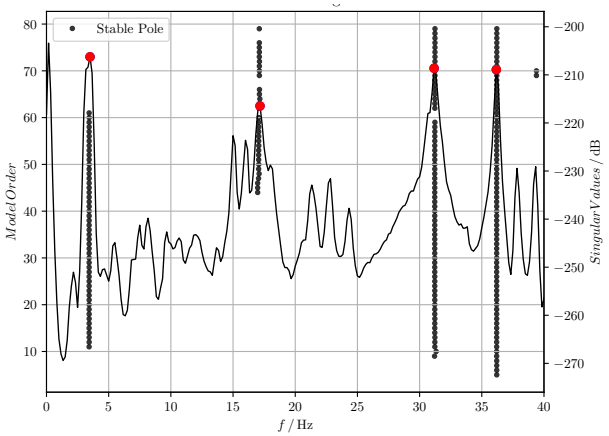

Fig. 8: Stability diagram and singular value spectrum of OMA performed on two axis of the Grenobler Bridge.

The largest peaks of the singular value spectrum clearly correspond to the stable poles displayed on the stability diagram. All of these modes, however, seem to be bending modes since the signs of the mode shapes in vertical direction are equal at each. The modal displacements in the direction of the river show effects from the asymmetric design leading to significant horizontal movement. Taking measurements at more modal coordinates on the bridge should give more information and torsional modes should also be made visible. The results from EFDD and SSI-COV are listed in table III.

Method	f_n / Hz	ζ / %	MPC
SSI-COV	3.43	5.34	1.00
	17.09	1.10	0.99
	31.21	0.73	0.41
	36.20	0.27	0.71
EFDD	3.58	6.13	0.99
	17.15	0.22	0.09
	31.25	0.81	1.00
	36.21	0.33	1.00

TABLE III: Comparison of modal parameters between OMA methods performed on the Grenobler Bridge.

The tests performed on the Grenobler bridge do not seem to show big improvements in terms of ease of identification, even though the loads from traffic are a lot higher than the ones on the Tiflis Bridge.

VI. Conclusion

The results of OMA performed on the two measurements of the Tiflis Bridge show that modal analysis of infrastructure using the output only approach works. The quality of results, however, heavily depends on the natural excitation present at each day. Influences like differences in currents of the river flowing under the bridge, wind strength and the intensity of traffic can skew the results. When the natural excitation covers a broad band of frequencies without containing too many harmonic components, the process of identifying physical modes with the help of the singular value spectrum as well as the stability diagram generated from SSI is relatively straight forward. If the forces on the structure only excite certain frequencies or modes, the process can be very tedious for the user. In general it seems good practice on bridge like structures to artificially improve excitation by applying impacts random in time and space. If impacts are not an option when carrying out the measurements, OMA is still possible

but the selection of physical modes heavily relies on the knowledge of the conducting engineer about structural dynamics and realistic mode shapes for these structures. For bridges, which are beam-like in shape the modes follow certain patterns, where for bending modes a zero-crossing is added each mode.

Comparing the results of frequency- and time domain methods one can conclude that except for the differences in damping estimation, which even for traditional methods like EMA is not very reliable, both work well to extract the modal parameters. The peak picking technique used for EFDD relies more on the experience and existing knowledge of the user since the peaks do not always correspond to physical modes. That is why a combination of both methods seems to be the ideal approach, though, this corresponds to an increase in computational effort.

As for the the comparison with EMA, OMA definitely has its advantages. An infrastructure building can never be completely isolated from all forces acting on it. Hence the calculation of modal parameters using EMA is always biased. For very large buildings the excitation sources have to be capable of producing immense forces for the structure to be excited in a sufficient manner. These technical solutions are not necessary for OMA. The disadvantages of output only modal analysis, however, are the increased measurement times and the need for more sensors, since references are necessary.

One could now conclude that the ideal approach for performing OMA on a bridge is to measure the building with added excitation, if feasible, and during processing combine EFDD with SSI to reliably choose the physical modes of the structure.

ACKNOWLEDGMENT

I would like to acknowledge the support from my supervisor, Dr. techn. Franz-Josef Falkner, and thank him for the performing the EMA on the Tiflis Bridge to validate OMA. My gratitude also extends to Matthias Panny, M.Sc. for helping me with the field experiments on the Grenobler Bridge.

Special thanks goes to Rune Brincker, whose published work provides sheer endless information on the topic at hand.

Finally, thanks goes to the Management Center Innsbruck for enabling this work.

REFERENCES

[1] R. Brincker and C. E. Ventura, *Introduction to Operational Modal Analysis*. Chichester: John Wiley & Sons, 2015.

[2] R. Brincker and P. Andersen, "Method for vibration analysis," Patent US 6,779,404 B1, aug 24, 2004, united States patent.

[3] R. Brincker, C. E. Ventura, and P. Andersen, "Damping estimation by frequency domain decomposition," in *Proceedings of IMAC 19: A Conference on Structural Dynamics*. Hyatt Orlando, Kissimmee, Florida: Society for Experimental Mechanics, 2001, pp. 698–703.

[4] D. J. Ewins, *Modal Testing: Theory, Practice, and Application*. Letchworth: Research Studies Press, 2000.

[5] Y. Xie, P. Liu, and G.-P. Ca, "Modal parameter identification of flexible spacecraft using the covariance-driven stochastic subspace identification (ssi-cov) method," in *Acta Mech. Sin. (2016) 32(4)*. The Chinese Society of Theoretical and Applied Mechanics, 2016, pp. 710–719.

[6] R. Brincker and P. Andersen, "Understanding stochastic subspace identification," in *IMAC-XXIV: A Conference & Exposition on Structural Dynamics*. Society for Experimental Mechanics, 2006, pp. 461–466.

[7] S. Chauhan, "Subspace algorithms in modal parameter estimation for operational modal analysis: Perspectives and practices," Bruel & Kjær Sound and Vibration Measurement A/S, Skodsborgvej, Tech. Rep., 2016.

[8] T. Kainz. Architektonisch ansprechend: Die neue grenobler brücke. [Online]. Available: https://www.meinbezirk.at/innsbruck/c-lokales/architektonisch-ansprechend-die-neue-grenobler-bruecke_a2593616

Markus Klötzer takes the Master's degree program Mechatronics - Smart Technologies with focus on mechanical engineering at the Management Center Innsbruck. During the Master's courses his focus shifted slightly from automation and robotics to structural dynamics with his thesis focusing on the topic of operational modal analysis.